NASA CR-66572

AERO-ASTRONAUTICS REPORT NO. 34

CONICAL BODIES OF GIVEN LENGTH AND VOLUME

HAVING MAXIMUM LIFT-TO-DRAG RATIO

AT HYPERSONIC SPEEDS:

DIRECT METHODS

by

ANGELO MIELE, JOHN C. HEIDEMAN, and ROBERT E. PRITCHARD

RICE UNIVERSITY

1967

CONICAL BODIES OF GIVEN LENGTH AND VOLUME

HAVING MAXIMUM LIFT-TO-DRAG RATIO AT HYPERSONIC SPEEDS:

DIRECT METHODS[1]

by

ANGELO MIELE[2], JOHN C. HEIDEMAN[3], and ROBERT E. PRITCHARD[4]

SUMMARY

An investigation of the lift-to-drag ratio attainable by a slender, conical body

flying at hypersonic speeds is presented under the assumptions that the pressure

distribution is modified Newtonian and the surface-averaged friction coefficient is

constant. The length and the volume are given, and the values of the free-stream

dynamic pressure, the factor modifying the Newtonian pressure distribution, and

the surface-averaged friction coefficient are known a priori. Direct methods are

employed throughout the paper.

First, the following two-parameter families of transversal contours are

analyzed: (a) flat-top triangle, (b) flat-top semiellipse, (c) flat-top rectangle, (d) flat-

bottom triangle, (e) flat-bottom semiellipse, (f) flat-bottom rectangle. For each of

these families, the combination of height and width yielding the maximum lift-to-drag

ratio is found. Regardless of the prescribed length and volume, the flat-bottom

triangle is aerodynamically superior to the other configurations. An upper bound

to the lift-to-drag ratio E exists and is given by $E = 0.529 \sqrt[3]{(n/C_f)}$, where C_f is the

surface-averaged friction coefficient and n is the factor modifying the Newtonian pressure

law. Therefore, for $C_f = 10^{-3}$ and n = 1, the highest attainable lift-to-drag ratio is

E = 5.29.

Next, the following two-parameter families, endowed with particular aerodynamic

properties, are analyzed: (g) bodies having minimum local drag, (h) bodies having

maximum local lift, and (i) bodies having maximum local lift-to-drag ratio. It is shown

that shapes (g) and (i) are aerodynamically inferior to the flat-bottom triangle. Shape

(h) is slightly superior to the flat-bottom triangle for relatively small volumes but

inferior for relatively large volumes.

Finally, the following three-parameter families of transversal contours are

analyzed: (j) diamond shape and (k) lenticular shape. These shapes are superior to

shapes (a) through (i) even though the improvement in the lift-to-drag ratio over that

of the flat-bottom triangle is small. The lenticular shape is slightly better than the

diamond shape, and its geometry approximates closely that of the variational solution

1. INTRODUCTION

In Ref. 1, the lift-to-drag ratio obtainable by a slender, homothetic body at hypersonic speeds was studied under the assumptions that the pressure coefficient is modified Newtonian and the surface-averaged friction coefficient is constant. Attention was given to configurations whose length is given, whose volume is unconstrained, and whose cross-sectional elongation ratio is prescribed.

In this report, we study the problem complementary to that investigated in Ref. 1, that of configurations whose length and volume are given, while the cross-sectional elongation ratio is free. Since the main objective is to study the effect of the transversal contour on the lift-to-drag ratio, the longitudinal contour is assumed conical for all cases. The following hypotheses are employed: (a) the body is conical, (b) the body is longitudinally slender, (c) a plane of symmetry exists between the left-hand and right-hand sides of the body, (d) the base plane is perpendicular to the plane of symmetry, (e) the free-stream velocity is contained in the plane of symmetry and is perpendicular to the base plane, (f) the pressure distribution is modified Newtonian, that is, the pressure coefficient is proportional to the cosine squared of the angle between the local normal to the body and the undisturbed flow direction, (g) the surface-averaged friction coefficient is constant, (h) the base drag coefficient is zero, and (i) the contribution of the tangential forces to the lift is negligible with respect to the contribution of the normal forces.

2.   LIFT-TO-DRAG RATIO

Consider the Cartesian coordinate system Oxyz and the cylindrical coordinate

system $Oxr\theta$ shown in Fig. 1. For the Cartesian system, the origin O is at the apex

of the body. the x-axis is parallel to the free-stream velocity and positive toward the

base, the z-axis is contained in the plane of symmetry and positive downward, and the

y-axis is oriented in such a way that the xyz-system is right-handed. For the cylindrical

system, r is the distance of any point from the x-axis, and θ measures the angular

position of the vector $\vec{r}$ with respect to the xy-plane.

The geometry of an arbitrary body in the cylindrical coordinate system can be

written in the form

$$r = r(x, \theta) \tag{1}$$

Therefore, if all the hypotheses of the introduction are employed, except hypothesis (a),

the drag D and lift L per unit free-stream dynamic pressure q_∞ can be written as (Ref. 1)

$$D/q_\infty = \int_0^\ell \int_{-\pi/2}^{\pi/2} [4nr^3 r_x^3/(r^2+r_\theta^2)+2C_f/(r^2+r_\theta^2)] \, dxd\theta$$

$$\tag{2}$$

$$L/q_\infty = \int_0^\ell \int_{-\pi/2}^{\pi/2} [4nr^2 r_x^2/(r^2+r_\theta^2)] (r \sin \theta - r_\theta \cos \theta) \, dxd\theta$$

where ℓ denotes the length of the body. C_f the surface-averaged friction coefficient,

and n a factor modifying the Newtonian pressure law[5].

If the body is conical, Eq. (1) has the form

$$r = R \, x/\ell \tag{3}$$

---

[5] Under the slender-body approximation, the pressure coefficient employed in Eqs. (2)
is given by $C_p = 2nr^2 r_x^2/(r^2 + r_\theta^2)$.

where $R = R(\theta)$ is the function describing the base contour. After the right-hand sides of Eqs. (2) are integrated in the longitudinal sense, the following results are obtained:

$$D/q_\infty = \int_{-\pi/2}^{\pi/2} [2nR^6/\ell^2(R^2 + \dot{R}^2) + C_f\ell_\wedge/(R^2 + \dot{R}^2)]\,d\theta$$

(4)

$$L/q_\infty = \int_{-\pi/2}^{\pi/2} [2nR^4/\ell(R^2 + \dot{R}^2)](R\sin\theta - \dot{R}\cos\theta)\,d\theta$$

where $\dot{R}$ denotes the derivative $dR/d\theta$.

If one introduces the constant

$$f = \sqrt[3]{(C_f/n)}$$

(5)

and the dimensionless quantities

$$\rho = R/\ell f, \quad D_* = D/nq_\infty\ell^2 f^4, \quad L_* = L/nq_\infty\ell^2 f^3$$

(6)

the previous relations become

$$D_* = \int_{-\pi/2}^{\pi/2} [2\rho^6/(\rho^2 + \dot{\rho}^2) + \sqrt{}/(\rho^2 + \dot{\rho}^2)]\,d\theta$$

(7)

$$L_* = \int_{-\pi/2}^{\pi/2} [2\rho^4/(\rho^2 + \dot{\rho}^2)](\rho\sin\theta - \dot{\rho}\cos\theta)\,d\theta$$

After the lift-to-drag ratio E and the modified lift-to-drag ratio E_* are defined as

$$E = L/D, \quad E_* = Ef$$

(8)

one obtains the relationship

$$E_* = L_*/D_* \qquad (9)$$

Clearly, the modified lift-to-drag ratio is uniquely determined once the dimensionless

base radius function $\rho(\theta)$ is prescribed.

3. BASE AREA AND VOLUME

Regardless of whether or not the body is slender, the base area and the volume are given by

$$S = \int_{-\pi/2}^{\pi/2} R^2 d\theta \ , \qquad\qquad V = \int_0^{\ell} \int_{-\pi/2}^{\pi/2} r^2 dx d\theta \qquad (10)$$

In particular, if the body is conical, Eqs. (10) become

$$S = 3V/\ell = \int_{-\pi/2}^{\pi/2} R^2 d\theta \qquad (11)$$

Therefore, prescribing the length and the base area is equivalent to prescribing the volume; conversely, prescribing the length and the volume is equivalent to prescribing the base area. After the dimensionless area S_* and the dimensionless volume V_* are defined as

$$S_* = S/\ell^2 f^2 \ , \qquad\qquad V_* = V/\ell^3 f^2 \qquad (12)$$

one concludes that

$$S_* = 3V_* = \int_{-\pi/2}^{\pi/2} \rho^2 d\theta \qquad (13)$$

4.   OPTIMUM TRANSVERSAL CONTOUR PROBLEM

We assume that the length ℓ and the volume V (and, hence, the base area S) are given. We also assume that the free-stream conditions are prescribed and that the quantities n and C_f are known a priori. Therefore, the dimensionless area S_* is known a priori. For each value of S_*, there exist an infinite number of cross-sectional shapes $\rho(\theta)$ which satisfy the isoperimetric constraint (13). Among these, it is of interest to find the one which maximizes the modified lift-to-drag ratio (9), where D_* and L_* are given by Eqs. (7).

Since the analysis of this problem with the indirect methods of the calculus of variations is considerably complicated, we postpone its solution to a subsequent report. Here, we present an introductory analysis based on direct methods. Specifically, we consider bodies whose base sections are of the type shown in Fig. 2. Here, O denotes the projection of the apex of the conical body on the base section, I is the maximum width point, and F is the point at which $\theta = \pi/2$. These cross sections include an upper contour OI which is rectilinear[6] and a lower contour IF whose equation $\rho = \rho(\theta)$ is to be specified; hence, these cross sections are described by

$$\rho = 0 \quad , \quad -\pi/2 \le \theta \le \theta_i$$

$$\dot{\rho} = \infty \quad , \qquad \theta = \theta_i \qquad\qquad (14)$$

$$\rho = \rho(\theta) \, , \qquad \theta_i \le \theta \le \pi/2$$

---

[6] An exception is the flat-bottom semiellipse.

Note that the upper contour has zero pressure drag, positive friction drag, and zero lift and that the lower contour has positive pressure drag, friction drag , and lift. With this understanding, the dimensionless drag, lift, area, and volume become

$$D_* = \rho_i + \int_{\theta_i}^{\pi/2} [2\rho^6/(\rho^2 + \dot\rho^2) + \sqrt{(\rho^2 + \dot\rho^2)}]\,d\theta$$

$$L_* = \int_{\theta_i}^{\pi/2} [2\rho^4/(\rho^2 + \dot\rho^2)](\rho \sin\theta - \dot\rho \cos\theta)\,d\theta \qquad (15)$$

$$S_* = 3V_* = \int_{\theta_i}^{\pi/2} \rho^2 d\theta$$

5. TWO-PARAMETER FAMILIES

Here, we consider a two-parameter family of transversal contours having

the form

$$\rho = \rho(\theta, \pi_1, \pi_2), \quad \theta_i \le \theta \le \pi/2 \qquad (16)$$

where

$$\theta_i = \theta_i(\pi_1, \pi_2) \qquad (17)$$

For this family, the integrals (15) are given by

$$D_* = D_*(\pi_1, \pi_2), \quad L_* = L_*(\pi_1, \pi_2), \quad S_* = S_*(\pi_1, \pi_2) \qquad (18)$$

and, as a consequence, the modified lift-to-drag ratio E_* depends on π_1 and π_2.

Among the combinations of π_1 and π_2 which satisfy the isoperimetric constraint (18-3),

we seek the pair which maximizes the ratio $E_* = L_*/D_*$. Standard methods of the theory

of maxima and minima show that the extremal solution is governed by the relationships

$$\partial F/\partial \pi_1 = 0, \quad \partial F/\partial \pi_2 = 0 \qquad (19)$$

where F denotes the fundamental function

$$F = L_* + \lambda_1 D_* + \lambda_2 S_* \qquad (20)$$

and where λ_1 and λ_2 are undetermined, constant Lagrange multipliers. Upon eliminating

the multiplier λ_2 between Eqs. (19), solving for λ_1, and recalling that $\lambda_1 + E_* = 0$,

we deduce that

$$\frac{L_*(\pi_1, \pi_2)}{D_*(\pi_1, \pi_2)} = \frac{J(L_*, S_*/\pi_1, \pi_2)}{J(D_*, S_*/\pi_1, \pi_2)} \tag{21}$$

where the symbol J stands for Jacobian determinant. Equations (18-3) and (21) admit solutions of the form

$$\pi_1 = \pi_1(S_*) \ , \ \ \pi_2 = \pi_2(S_*) \tag{22}$$

Once π_1 and π_2 are known, the dimensionless lift and drag can be computed with Eqs. (18-1) and (18-2) and the modified lift-to-drag ratio

$$E_* = E_*(S_*) \tag{23}$$

with Eq. (9).

5.1. Flat-Top Bodies. As a first step, bodies with the upper surface flat and parallel to the flow are considered. For these bodies, the parameters π_1 and π_2 are chosen to be

$$\pi_1 = \rho_i \ , \ \ \pi_2 = \rho_f \tag{24}$$

The following two-parameter shapes are analyzed: (a) flat-top triangle, (b) flat-top semiellipse, and (c) flat-top rectangle. For each shape, the optimum values of the functions

$$\rho_i = \rho_i(S_*) \ , \qquad \rho_f = \rho_f(S_*) \ , \qquad E_* = E_*(S_*) \tag{25}$$

have been calculated using an IBM 7040 computer and are plotted in Figs. 3 through 5.

Shown in Fig. 6 is the cross-sectional elongation ratio

$$\alpha = \rho_i / \rho_f \tag{26}$$

and, in Fig. 7, the optimum contours for $S_* = 3$.

As Fig. 5 shows, for relatively low values of S_*, the rectangular cross section is aerodynamically more efficient than the other two; while, for relatively high values of S_*, the triangular cross section is the best. For each shape, a value of the dimensionless area S_* exists which yields the highest lift-to-drag ratio. This value is given in Table 1 together with the associated initial radius, final radius, lift-to-drag ratio, and elongation ratio.

Table 1

Cross section	S_*	ρ_i	ρ_f	E_*	α
Triangular	∞	∞	1.260	0.529	∞
Semielliptical	2.317	1.469	1.004	0.367	1.467
Rectangular	1.978	0.630	1.570	0.366	0.401

The conclusions of this section are qualitatively consistent with the wind-tunnel tests reported by Whitehead in Ref. 2. Whitehead, who investigated conical configurations having given length, volume, and elongation ratio at $M = 6.9$ and $S_* \cong 3$, found that the flat-top triangle is aerodynamically superior to the flat-top semiellipse and the flat-top rectangle. However, this comparison should be viewed cum grano salis,

since the elongation ratio was kept constant in Ref. 2, while it has been optimized

in the present analysis.

5.2. <u>Flat-Bottom Bodies</u>. As a second step, bodies with the lower surface flat

and inclined with respect to the flow are considered. For these bodies, the parameters

π_1 and π_2 can be chosen as in Eqs. (24). The following two-parameter shapes are

analyzed: (d) flat-bottom triangle, (e) flat-bottom semiellipse, and (f) flat-bottom

rectangle. For each shape, the optimum values of the functions (25) have been calculated

using an IBM 7040 computer and are plotted in Figs. 8 through 10. Shown in Fig. 11

is the initial angle θ_i and, in Fig. 12, the cross-sectional elongation ratio

$$\alpha = \rho_i \cos \theta_i / \rho_f \qquad (27)$$

Next, Fig. 13 shows the optimum contours for $S_* = 3$.

As Fig. 10 shows, regardless of the dimensionless area S_*, the flat-bottom

triangle is more efficient than the flat-bottom semiellipse and the flat-bottom rectangle.

For each shape, a value of the dimensionless area S_* exists which yields the highest

lift-to-drag ratio. This value is given in Table 2 together with the associated initial

radius, final radius, lift-to-drag ratio, initial angle, and elongation ratio.

Table 2

Cross section	S_*	ρ_i	ρ_f	E_*	θ_i (degrees)	α
Triangular	∞	∞	1.260	0.529	0	∞
Semielliptical	1.797	1.647	1.444	0.411	61.31	0.548
Rectangular	1.978	0.630	1.570	0.366	68.18	0.401

The conclusions of this section are qualitatively consistent with the wind-tunnel tests

reported by Whitehead in Ref. 2. Whitehead, who investigated conical configurations

having given length, volume, and elongation ratio at $M = 6.9$ and $S_* \cong 3$, found that

the flat-bottom triangle is aerodynamically superior to the flat-bottom semiellipse

and the flat-bottom rectangle. Comparison of the flat-bottom triangle with the flat-top

triangle shows that the former is superior to the latter regardless of the value of the

dimensionless area S_*. An analogous remark holds if the flat-bottom triangle is

compared with the flat-top semiellipse and the flat-top rectangle. These conclusions

are consistent with Whitehead's wind-tunnel tests (Ref. 2).

5.3. Bodies Locally Optimum Aerodynamically[7]. As a third step, bodies whose

lower contour is endowed with particular aerodynamic properties are considered,

specifically: (g) bodies having minimum local drag, (h) bodies having maximum local

lift, and (i) bodies having maximum local lift-to-drag ratio. Contour (g) is obtained by

minimizing the integrand in Eq. (15-1) with respect to $\dot{\rho}$ for constant values of ρ and θ.

Contour (h) is obtained by maximizing the integrand in Eq. (15-2) with respect to $\dot{\rho}$ for

constant values of ρ and θ. And contour (i) is obtained by maximizing the ratio of the

integrand in Eq. (15-2) to the integrand in Eq. (15-1) with respect to $\dot{\rho}$ for constant

values of ρ and θ. Each contour is described by a first-order differential equation of

the form

$$\dot{\rho} = A(\theta, \rho) \tag{28}$$

---

[7] The data of this section have been obtained by graphical interpolation.

which, upon backward integration from the final point, yields the function

$$\rho = B(\theta, \rho_f) \tag{29}$$

As a consequence, the relation

$$\rho_i = B(\theta_i, \rho_f) \tag{30}$$

holds at the initial point. The associated dimensionless area is given by

$$S_* = - \int_{\pi/2}^{\theta_i} B^2(\theta, \rho_f) \, d\theta \tag{31}$$

Clearly, a particular body of type (g), (h), or (i) can be identified by two parameters, for instance, ρ_f and θ_i, ρ_f and ρ_i, or ρ_i and θ_i. Regardless of the description employed, the solution of the optimization problem leads to the results summarized in Figs. 14 through 18. Also shown in Fig. 19 are the optimum contours for $S_* = 3$.

As Fig. 16 shows, shapes of type (g) are rather poor from an aerodynamic point of view. For relatively low values of S_*, shape (h) is more efficient than shape (i), while the opposite is true for relatively high values of S_*. For each shape, a value of the dimensionless area S_* exists which yields the highest lift-to-drag ratio. This value is given in Table 3 together with the associated initial radius, final radius, lift-to-drag ratio, initial angle, and elongation ratio.

Table 3

Cross section	S_*	ρ_i	ρ_f	E_*	θ_i (degrees)	α
Minimum local drag	∞	∞	0.63	0.318	0	∞
Maximum local lift	1.75	1.55	1.22	0.491	31	1.1
Maximum local lift-to-drag ratio	72.4	70.0	1.07	0.502	6	65.0

Comparison of shape (h) with the flat-bottom triangle shows that the former is superior to the latter for $S_* < 1.2$, while the opposite is true for $S_* > 1.2$. On the other hand, shape (i) is aerodynamically inferior to the flat-bottom triangle for every value of S_*.

6.   THREE-PARAMETER FAMILIES

Here, we consider a three-parameter family of transversal contours having the form

$$\rho = \rho(\theta, \pi_1, \pi_2, \pi_3) \, , \quad \theta_i \leq \theta \leq \pi/2 \tag{32}$$

where

$$\theta_i = \theta_i(\pi_1, \pi_2, \pi_3) \tag{33}$$

For this family, the integrals (15) are given by

$$D_* = D_*(\pi_1, \pi_2, \pi_3) \, , \quad L_* = L_*(\pi_1, \pi_2, \pi_3), \quad S_* = S_*(\pi_1, \pi_2, \pi_3) \tag{34}$$

and, as a consequence, the modified lift-to-drag ratio E_* depends on π_1, π_2, π_3. Among the combinations of π_1, π_2, π_3 which satisfy the isoperimetric constraint (34-3), we seek the triplet which maximizes the ratio $E_* = L_*/D_*$. Standard methods of the theory of maxima and minima show that the extremal solution is governed by the relationships

$$\partial F/\partial \pi_1 = 0, \quad \partial F/\partial \pi_2 = 0, \quad \partial F/\partial \pi_3 = 0 \tag{35}$$

where F denotes the fundamental function

$$F = L_* + \lambda_1 D_* + \lambda_2 S_* \tag{36}$$

and where λ_1 and λ_2 are undetermined, constant Lagrange multipliers. Upon eliminating the multiplier λ_2 among Eqs. (35), solving for λ_1, and recalling that $\lambda_1 + E_* = 0$,

we deduce that

$$\frac{L_*(\pi_1,\pi_2,\pi_3)}{D_*(\pi_1,\pi_2,\pi_3)} = \frac{J(L_*,S_*/\pi_1,\pi_2)}{J(D_*,S_*/\pi_1,\pi_2)} = \frac{J(L_*,S_*/\pi_2,\pi_3)}{J(D_*,S_*/\pi_2,\pi_3)} \tag{37}$$

where the symbol J stands for Jacobian determinant. Equations (34-3) and (37) admit

solutions of the form

$$\pi_1 = \pi_1(S_*) \ , \quad \pi_2 = \pi_2(S_*) \ , \quad \pi_3 = \pi_3(S_*) \tag{38}$$

Once π_1, π_2, π_3 are known, the dimensionless lift and drag can be computed with Eqs. (34-1)

and (34-2) and the modified lift-to-drag ratio

$$E_* = E_*(S_*) \tag{39}$$

with Eq. (9).

6.1. Diamond and Lenticular Shapes. In this section, the following shapes are

discussed: (j) diamond shape and (k) lenticular shape. Contour (j) is made of straight

lines. Contour (k) is composed of two straight lines and a circular arc with center above

the apex. For these contours, the parameters π_1, π_2, π_3 are chosen to be

$$\pi_1 = \theta_i \ , \quad \pi_2 = \rho_i \ , \quad \pi_3 = \rho_f \tag{40}$$

For each cross-sectional shape, the optimum values of the functions

$$\theta_i = \theta_i(S_*) \ , \quad \rho_i = \rho_i(S_*) \ , \quad \rho_f = \rho_f(S_*) \ , \quad E_* = E_*(S_*) \ , \quad \alpha = \alpha(S_*) \tag{41}$$

have been calculated using an IBM 7040 computer and are plotted in Figs. 20 through 24.

Also shown in Fig. 25 are the optimum contours for $S_* = 3$.

Regardless of the value of S_*, the lift-to-drag ratio of the lenticular shape is higher than that of the diamond shape. However, the relative difference is so small that it cannot be shown in the scale in which Fig. 23 is drawn. Also regardless of the value of S_*, the diamond shape and the lenticular shape are more efficient aerodynamically than any of those analyzed previously. Analyses presently under way indicate that the geometry of the lenticular shape is quite close to that of the variational solution. As the dimensionless area S_* increases, the lift-to-drag ratio of the diamond shape and that of the lenticular shape increase, tending to the limiting value $E_* = 0.529$ when $S_* = \infty$. Under these limiting conditions, the elongation ratio is $\alpha = \infty$, that is, the configuration is winglike rather than bodylike.

7.   DISCUSSION AND CONCLUSIONS

In the previous sections, the optimization of the lift-to-drag ratio of a slender, conical body flying at hypersonic speeds is presented under the assumptions that the pressure distribution is modified Newtonian and the surface-averaged friction coefficient is constant. The length and volume are given, and the values of the free-stream dynamic pressure, the factor modifying the Newtonian pressure distribution, and the surface-averaged friction coefficient are known a priori. While the variational investigation of the optimum transversal contour is postponed to a subsequent paper, the effect of the main geometric parameters of a cross section on the lift-to-drag ratio is analyzed systematically with direct methods. Several two-parameter and three-parameter families of transversal contours are considered. It is shown that the optimum value of the modified lift-to-drag ratio E_* is a unique function of the dimensionless area S_*. With this understanding, the conclusions outlined below are reached.

Flat-Top Shapes. Three cross sections of this type are considered: (a) flat-top triangle, (b) flat-top semiellipse, and (c) flat-top rectangle. For each shape, the combination of height and width yielding the maximum lift-to-drag ratio is found. It is shown that, for relatively low values of S_*, cross section (c) is aerodynamically superior to the other two; while, for relatively high values of S_*, cross section (a) is the best. An upper bound to the lift-to-drag ratio is shown to exist and is given by $E_* = 0.529$. This value corresponds to a lift-to-drag ratio $E = 5.29$ when $C_f = 10^{-3}$ and $n = 1$.

Flat-Bottom Shapes. Three cross sections of this type are considered: (d) flat-bottom triangle, (e) flat-bottom semiellipse, and (f) flat-bottom rectangle. It is shown that,

regardless of the value of S_*, cross section (d) is not only aerodynamically superior

to shapes (e) and (f), but also to shapes (a) through (c).

Shapes Locally Optimum Aerodynamically. Three cross sections of this type

are considered: (g) contour having minimum local drag, (h) contour having maximum

local lift, and (i) contour having maximum local lift-to-drag ratio. It is shown that

shapes (g) and (i) are aerodynamically inferior to shape (d). Shape (h) is slightly superior

to shape (d) for relatively small values of S_* but inferior for relatively large values of S_*.

Diamond and Lenticular Shapes. In an attempt to improve the aerodynamic

characteristics of flat-bottom shapes, attention is given to (j) the diamond shape and

(k) the lenticular shape. It is shown that, regardless of the value of S_*, shapes (j)

and (k) are superior to contours (a) through (i). However, the lift-to-drag ratios of

shapes (j) and (k) are only slightly higher than that of shape (d). Also, shape (k) is

slightly better than shape (j) and its geometry approximates closely that of the variational

solution.

APPENDIX A. CROSS-SECTIONAL CHARACTERISTICS

In this appendix, we present a summary of the main characteristics of the cross

sections considered in Sections 5 and 6.

(a) <u>Flat-Top Triangle</u>, $\theta_i = 0$. The lower contour is given by

$$\rho = \rho_i \rho_f / (\rho_i \sin \theta + \rho_f \cos \theta), \quad \theta_i \le \theta \le \pi/2 \tag{42}$$

and the integrals (15) have the values

$$D_* = 2\rho_i^3 \rho_f^3 / (\rho_i^2 + \rho_f^2) + \rho_i + \sqrt{(\rho_i^2 + \rho_f^2)}$$

$$L_* = 2\rho_i^3 \rho_f^2 / (\rho_i^2 + \rho_f^2) \tag{43}$$

$$S_* = \rho_i \rho_f$$

(b) <u>Flat-Top Semiellipse</u>, $\theta_i = 0$. The lower contour is given by

$$\rho = \rho_i \rho_f / \sqrt{(\rho_i^2 \sin^2 \theta + \rho_f^2 \cos^2 \theta)}, \quad \theta_i \le \theta \le \pi/2 \tag{44}$$

and the integrals (15) have the values

$$D_* = \pi \rho_i^2 \rho_f^2 + \rho_i [1 + E(\pi/2, \, p/\rho_i)]$$

$$L_* = (\rho_i^2 \rho_f^2 / p) \log [(\rho_i + p)/(\rho_i - p)] \tag{45}$$

$$S_* = \pi \rho_i \rho_f / 2$$

where $p = \sqrt{(\rho_i^2 - \rho_f^2)}$ and where E denotes the complete elliptic integral of the second

kind.

(c) <u>Flat-Top Rectangle</u>, $\theta_i = 0$. The lower contour is given by

$$\rho = \rho_i/\cos\theta \qquad , \qquad \theta_i \leq \theta \leq \arctan(\rho_f/\rho_i)$$

(46)

$$\rho = \rho_f/\sin\theta \qquad , \qquad \arctan(\rho_f/\rho_i) \leq \theta \leq \pi/2$$

and the integrals (15) have the values

$$D_* = 2\rho_i\rho_f(\rho_i^2 + \rho_f^2) + \rho_f + 2\rho_i$$

$$L_* = 2\rho_i\rho_f^2$$

(47)

$$S_* = 2\rho_i\rho_f$$

(d) <u>Flat-Bottom Triangle</u>, $\theta_i = \arctan(\rho_f/\rho_i)$. The lower contour is given by

$$\rho = \rho_f/\sin\theta \qquad , \qquad \theta_i \leq \theta \leq \pi/2$$

(48)

and the integrals (15) have the values

$$D_* = 2\rho_f^3 p + \rho_i + p$$

$$L_* = 2\rho_f^2 p$$

(49)

$$S_* = \rho_f p$$

(e) <u>Flat-Bottom Semiellipse</u>. The upper contour is given by

$$\rho = 2\rho_f p^2 \sin\theta/(p^2\sin^2\theta + \rho_f^2\cos^2\theta) , 0 \leq \theta \leq \arcsin(\rho_f/\rho_i)$$

(50)

and the lower contour by

$$\rho = \rho_f/\sin\theta \quad , \quad \arcsin(\rho_f/\rho_i) \le \theta \le \pi/2 \tag{51}$$

The integrals (15) have the values

$$D_* = 2\rho_f^5 p/q^2 + \pi\rho_f^2 p^2(p + 4\rho_f)/(p + \rho_f) - 2\rho_f^3 p^2[(7\rho_f^2 - 3\rho_i^2)/q^3]\arctan(q/p)$$

$$+ p + \rho_f + (\rho_f - q)F(\varphi, k) - (\rho_f + q)[1 - E(\varphi, k)]$$

$$L_* = 2\rho_f^4 p/q^2 + 2\pi\rho_f^2 p^2/(p + \rho_f) - 2\rho_f^2 p^2[(3\rho_f^2 - \rho_i^2)/q^3]\arctan(q/p) \tag{52}$$

$$S_* = \pi\rho_f p/2$$

where $q = \sqrt{2\rho_f^2 - \rho_i^2})$. Here, F and E are the incomplete elliptic integrals of the first and second kind, whose argument φ and parameter k are given by

$$\varphi = \arctan[(\rho_f + q)/p]$$

$$\tag{53}$$

$$k = 2\sqrt{(\rho_f q)/(\rho_f + q)}$$

(f) <u>Flat-Bottom Rectangle</u>. See (c).

(g) <u>Shape of Minimum Local Drag</u>. The lower contour of this shape is described by the differential equation

$$(\partial/\partial\dot{\rho})[2\dot{\rho}^6/(\rho^2 + \dot{\rho}^2) + \sqrt{(\rho^2 + \dot{\rho}^2)}] = 0 \tag{54}$$

which is equivalent to

$$\dot{\rho} = 0 \quad \text{and/or} \quad \dot{\rho}^2 + \dot{\rho}^2 = (\rho\sqrt[3]{2})^4 \tag{55}$$

Upon integration, Eq. (15) leads to

$$\rho = C_1 \quad \text{and/or} \quad \rho \cos(C_2 - \theta) = \rho_o \tag{56}$$

where $\rho_o = 1/\sqrt[3]{4}$ and where C_1 and C_2 are constants. Equation (56-1) represents a

circular arc and Eq. (56-2) a straight line tangent to the circle of radius $\rho = \rho_o$.

The circular arc solution is valid providing $\rho \le \rho_o$ and the straight line solution,

providing $\rho \ge \rho_o$. Therefore, three classes of lower contours can be identified: (g-1)

circular arcs, (g-2) contours composed of straight lines tangent to the circle $\rho = \rho_o$,

and (g-3) contours composed of circular arcs of radius $\rho = \rho_o$ and straight lines tangent

to the circular arcs.

For contours (g-1), the integrals (15) take the values

$$D_* = C_1 + [2C_1^4 + C_1](\pi/2 - \theta_i)$$

$$L_* = 2C_1^3 \cos \theta_i \tag{57}$$

$$S_* = C_1^2(\pi/2 - \theta_i)$$

For contours (g-2), the integrals (15) take the values

$$D_* = \lceil \rho_o/\cos(C_2 - \theta_i)\rceil + (2\rho_o^4 + \rho_o)[\tan(C_2 - \theta_i) - \tan(C_2 - \pi/2)]$$

$$L_* = 2\rho_o^3 \sin C_2 [\tan(C_2 - \theta_i) - \tan(C_2 - \pi/2)] \tag{58}$$

$$S_* = \rho_o^2 [\tan(C_2 - \theta_i) - \tan(C_2 - \pi/2)]$$

And, for contours (g-3), the integrals (15) take the values

$$D_* = [\rho_o/\cos(C_2 - \theta_i)] + [2\rho_o^4 + \rho_o][(\pi/2 - C_2) + \tan(C_2 - \theta_i)]$$

$$L_* = 2\rho_o^3 \cos C_2 + 2\rho_o^3 \sin C_2 \tan (C_2 - \theta_i) \tag{59}$$

$$S_* = \rho_o^2(\pi/2 - C_2) + \rho_o^2 \tan (C_2 - \theta_i)$$

(h) Shape of Maximum Local Lift. The lower contour of this shape is described by the differential equation

$$(\partial/\partial\dot{\rho})\{[2\rho^4/(\rho^2 + \dot{\rho}^2)](\rho \sin \theta - \dot{\rho} \cos \theta)\} = 0 \tag{60}$$

which is equivalent to

$$\dot{\rho}/\rho = (\sin \theta - 1)/\cos \theta \tag{61}$$

Upon integration, Eq. (61) leads to

$$\rho = 2\rho_f/(1 + \sin \theta) \tag{62}$$

With this understanding, the integrals (15) take the values

$$D_* = \rho_i + 16\rho_f^4 \int_{\theta_i}^{\pi/2} (1 + \sin \theta)^{-3} d\theta + 2\sqrt{2}\, \rho_f \int_{\theta_i}^{\pi/2} (1 + \sin \theta)^{-3/2} d\theta$$

$$L_* = 8\rho_f^3 \int_{\theta_i}^{\pi/2} (1 + \sin \theta)^{-2} d\theta \tag{63}$$

$$S_* = 4\rho_f^2 \int_{\theta_i}^{\pi/2} (1 + \sin \theta)^{-2} d\theta$$

(i) <u>Shape of Maximum Local Lift-to-Drag Ratio.</u> The lower contour of this shape

is described by the differential equation

$$(\partial/\partial\dot\rho)\{2\rho^4(\rho\sin\theta - \dot\rho\cos\theta)/[2\rho^6 + \sqrt{(\rho^2 + \dot\rho^2)^3}]\} = 0 \qquad (64)$$

which is equivalent to

$$2\rho^6 + \sqrt{(\rho^2 + \dot\rho^2)^3} + 3\dot\rho(\rho\tan\theta - \dot\rho)\sqrt{(\rho^2 + \dot\rho^2)} = 0 \qquad (65)$$

and, upon differentiation, to

$$\ddot\rho = (P_1\sin\theta - P_2\cos\theta)/(P_3\sin\theta - P_4\cos\theta) \qquad (66)$$

where

$$P_1 = 2\rho^6\sqrt{(\rho^2 + \dot\rho^2)} + \rho^4 - 7\rho^2\dot\rho^2 - 5\dot\rho^4$$

$$P_2 = 3\rho\dot\rho[2\rho^2 + \dot\rho^2 + 4\rho^4\sqrt{(\rho^2 + \dot\rho^2)}]$$

$$(67)$$

$$P_3 = 3\rho(\rho^2 + 2\dot\rho^2)$$

$$P_4 = 3\dot\rho(\rho^2 + 2\dot\rho^2)$$

A characteristic of these shapes is that

$$\dot\rho_f = 0 \qquad (68)$$

With this understanding, the second-order differential equation (66) can be integrated

backward to obtain the function

$$\rho = A(\theta, \rho_f) \tag{69}$$

Once this function is known, the integrals (15) can be evaluated.

(j) <u>Diamond Shape</u>. The lower contour is given by

$$\rho = \rho_i \rho_f \cos \theta_i / [\rho_i \cos \theta_i \sin \theta + (\rho_f - \rho_i \sin \theta_i) \cos \theta] \tag{70}$$

and the integrals (15) have the values

$$D_* = 2\rho_i^3 \rho_f^3 \cos^3 \theta_i / r^2 + \rho_i + r$$

$$L_* = 2\rho_i^3 \rho_f^2 \cos^3 \theta_i / r^2 \tag{71}$$

$$S_* = \rho_i \rho_f \cos \theta_i$$

where $r = \sqrt{(\rho_i^2 + \rho_f^2 - 2\rho_i \rho_f \sin \theta_i)}$

(k) <u>Lenticular Shape</u>. The lower contour is given by

$$\rho = \{\sqrt{[(\rho_i^2 - \rho_f^2)^2 \sin^2 \theta + 2s^2 \rho_i \rho_f (\rho_i - \rho_f \sin \theta_i)]} - (\rho_i^2 - \rho_f^2) \sin \theta\} / s^2 \tag{72}$$

where $s = \sqrt{[2(\rho_f - \rho_i \sin \theta_i)]}$. For this shape, the integrals (15) have been evaluated numerically.

REFERENCES

1.   MIELE, A., and HUANG, H.Y., Lift-to-Drag Ratios of Lifting Bodies at

     Hypersonic Speeds, Rice University, Aero-Astronautics Report No. 29, 1967.

2.   WHITEHEAD, A.H., Jr., Effect of Body Cross Section and Width-Height Ratio

     on Performance of Bodies and Delta-Wing-Body Combinations at Mach 6.9,

     NASA TN No. D-2886, 1966.

LIST OF CAPTIONS

Fig. 1   Coordinate system.

Fig. 2   Cross sections analyzed.

Fig. 3   Initial radius.

Fig. 4   Final radius.

Fig. 5   Lift-to-drag ratio.

Fig. 6   Elongation ratio.

Fig. 7   Optimum contours for $S_* = 3$.

Fig. 8   Initial radius.
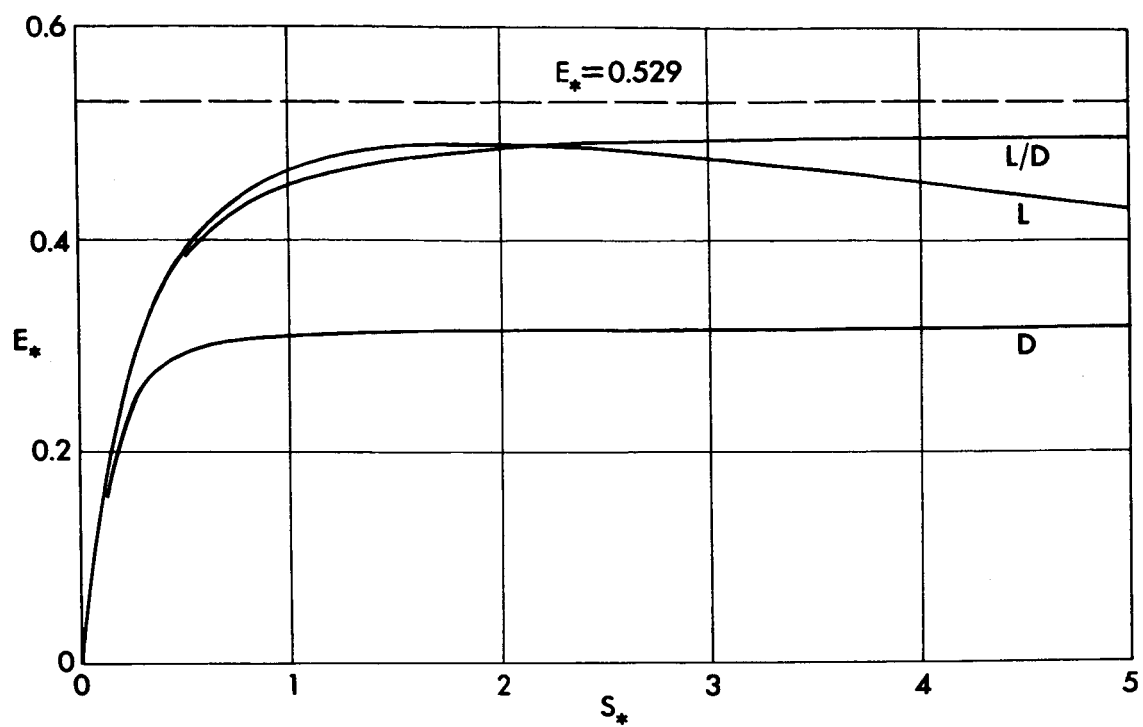
Fig. 9   Final radius.
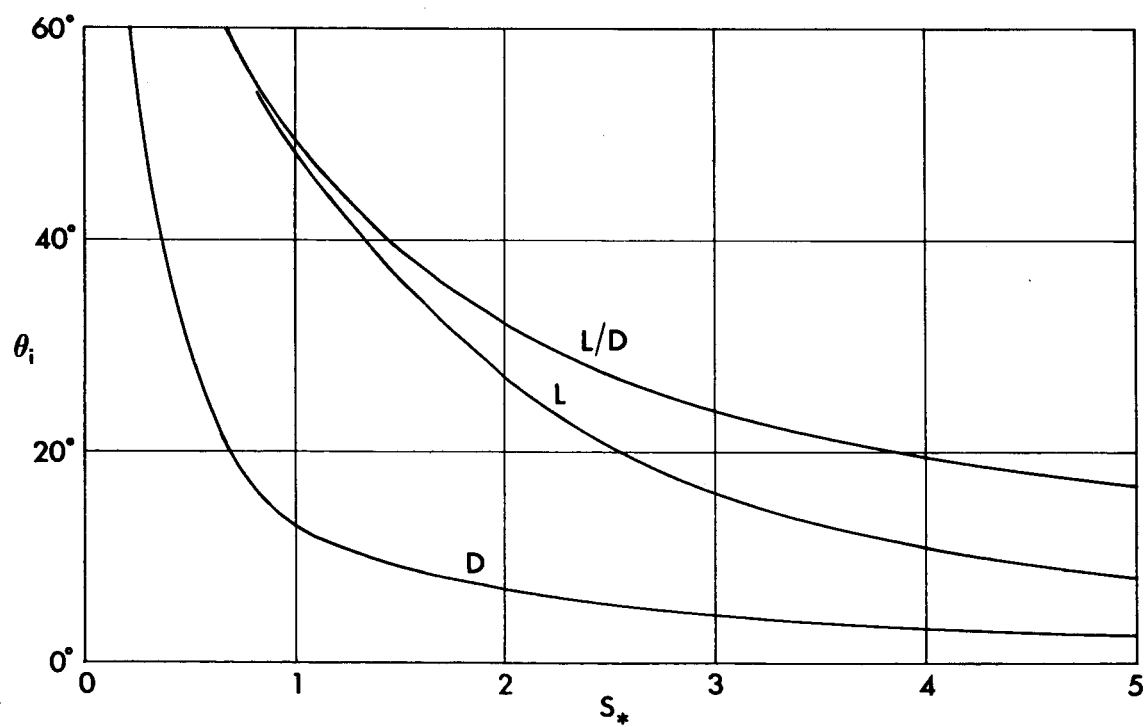
Fig. 10   Lift-to-drag ratio.

Fig. 11   Initial angle.

Fig. 12   Elongation ratio.

Fig. 13   Optimum contours for $S_* = 3$.

Fig. 14   Initial radius.

Fig. 15   Final radius.

Fig. 16   Lift-to-drag ratio.
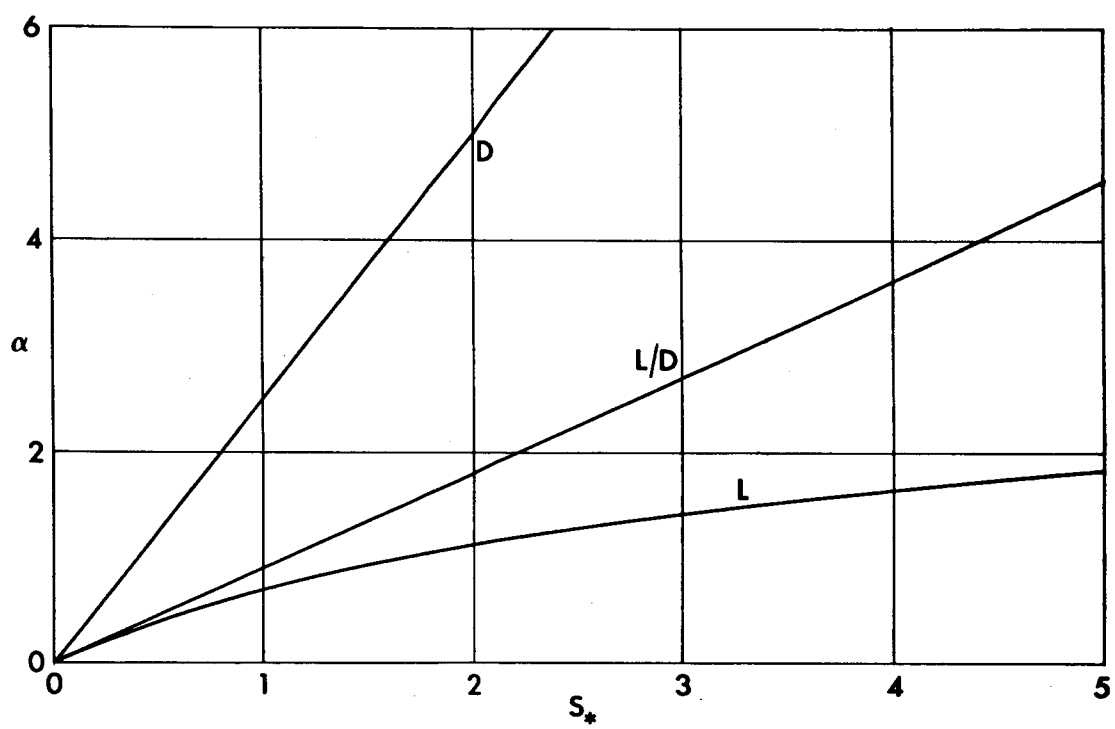
Fig. 17   Initial angle.
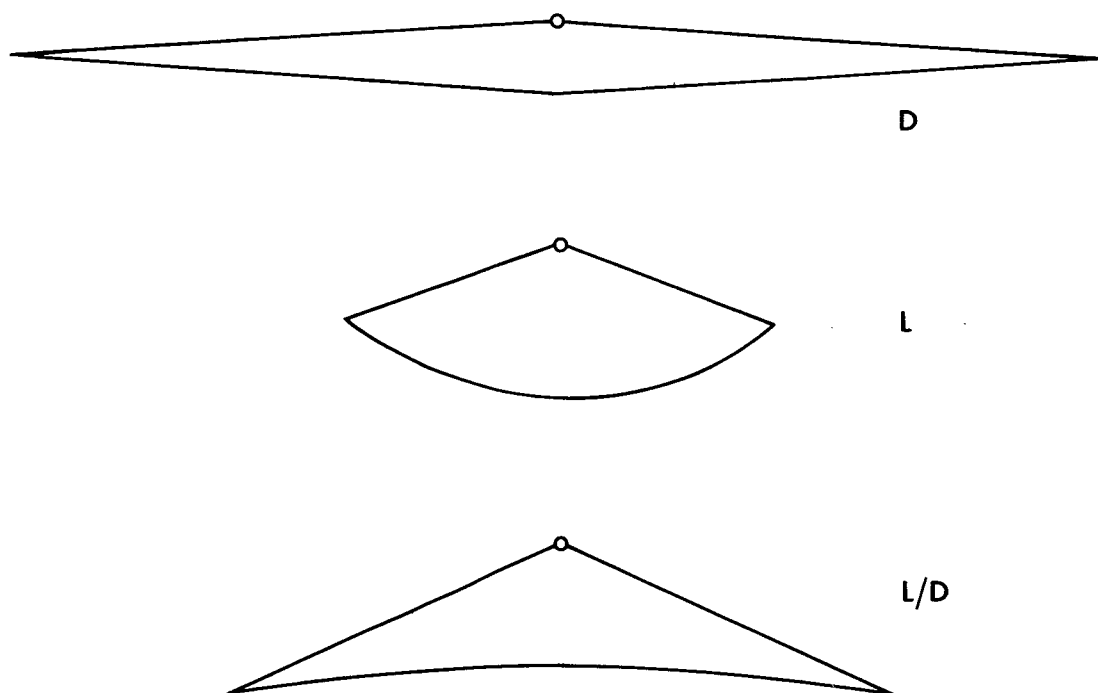
Fig. 18   Elongation ratio.
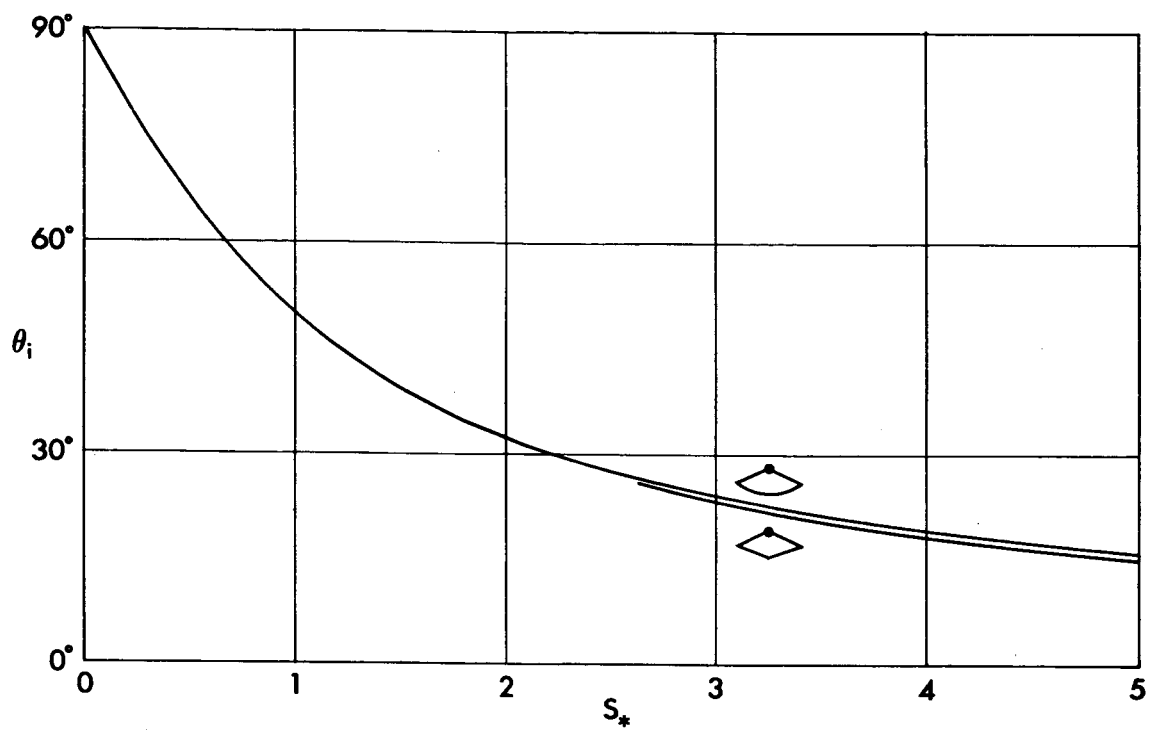
Fig. 19   Optimum contours for $S_* = 3$.

Fig. 20   Initial angle.

Fig. 21   Initial radius.

Undisturbed flow direction

Fig. 1   Coordinate system.

Fig. 5   Lift-to-drag ratio.
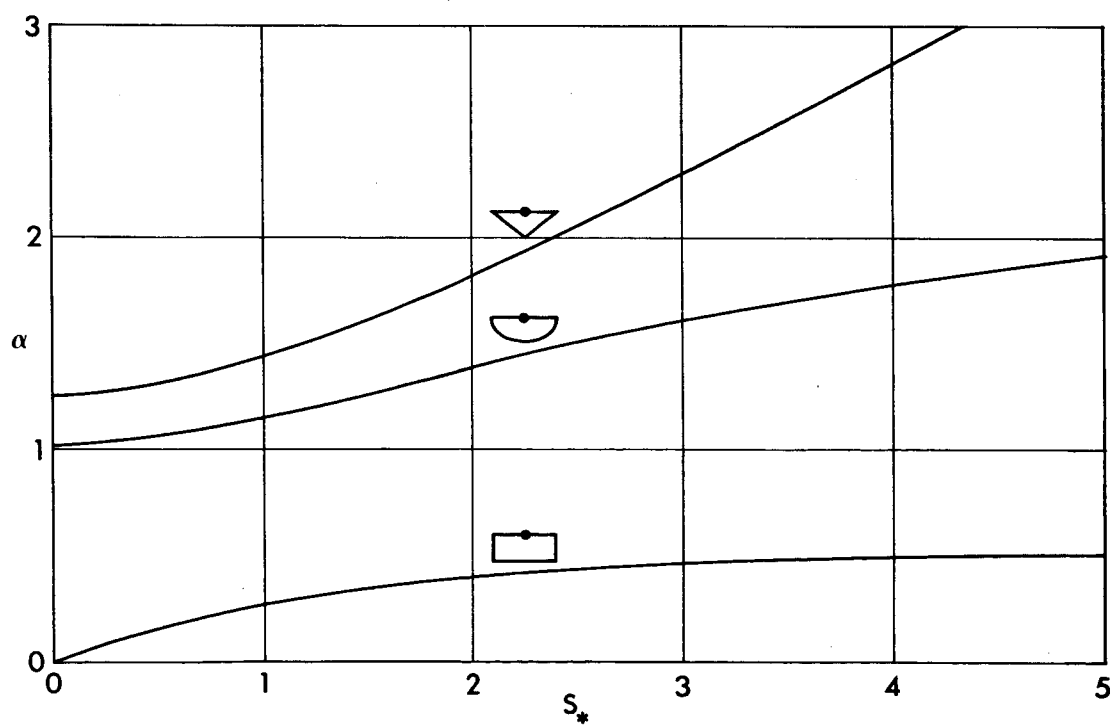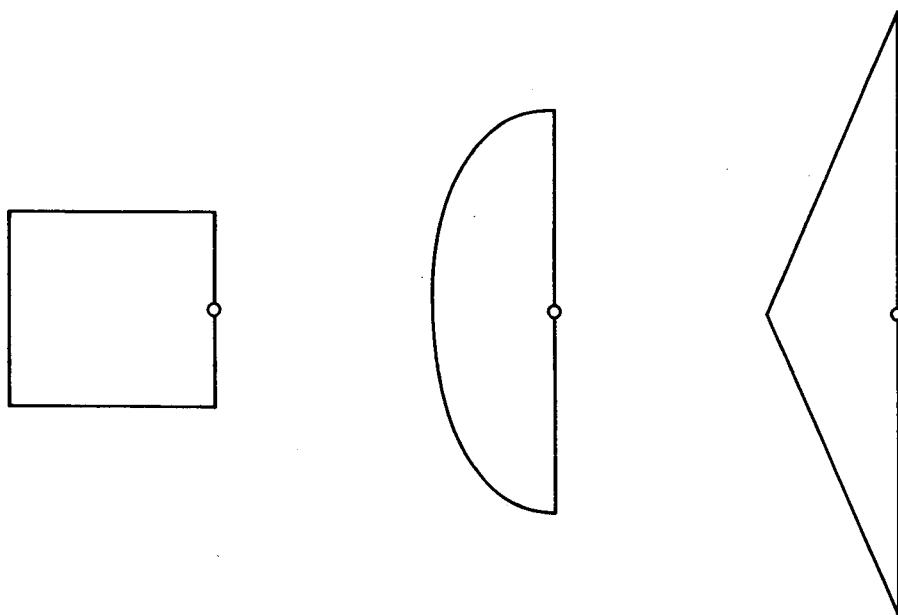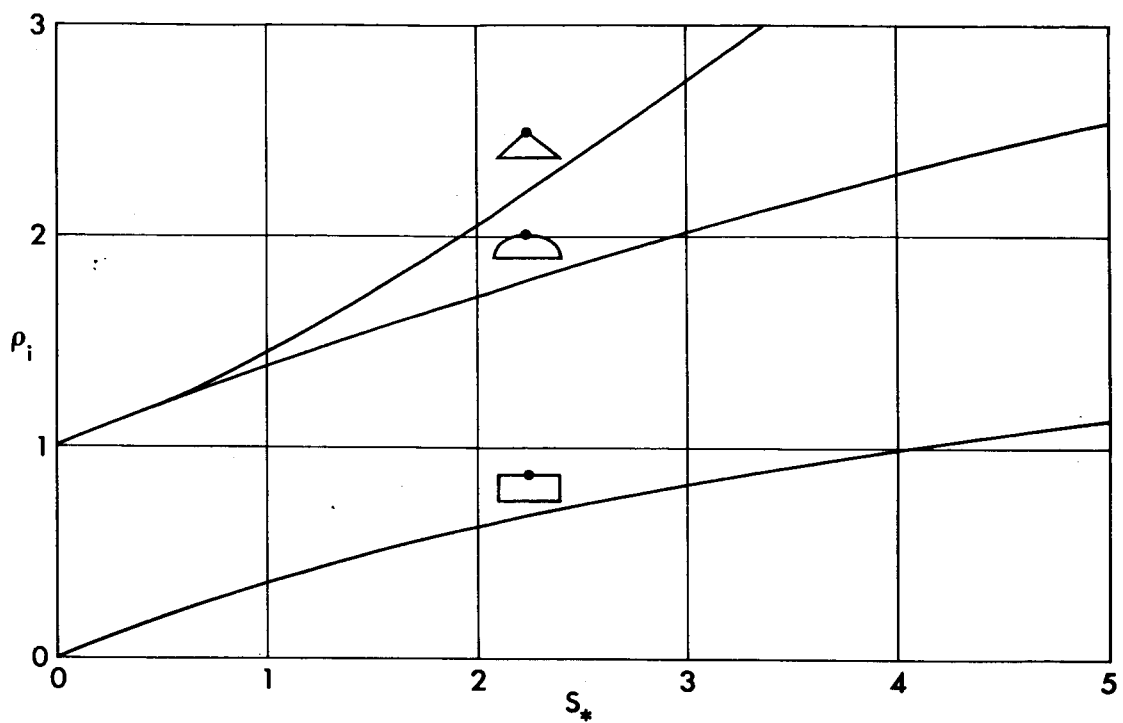
Fig. 6   Elongation ratio.

Fig. 7   Optimum contours for $S_* = 3$.

Fig. 8   Initial radius.
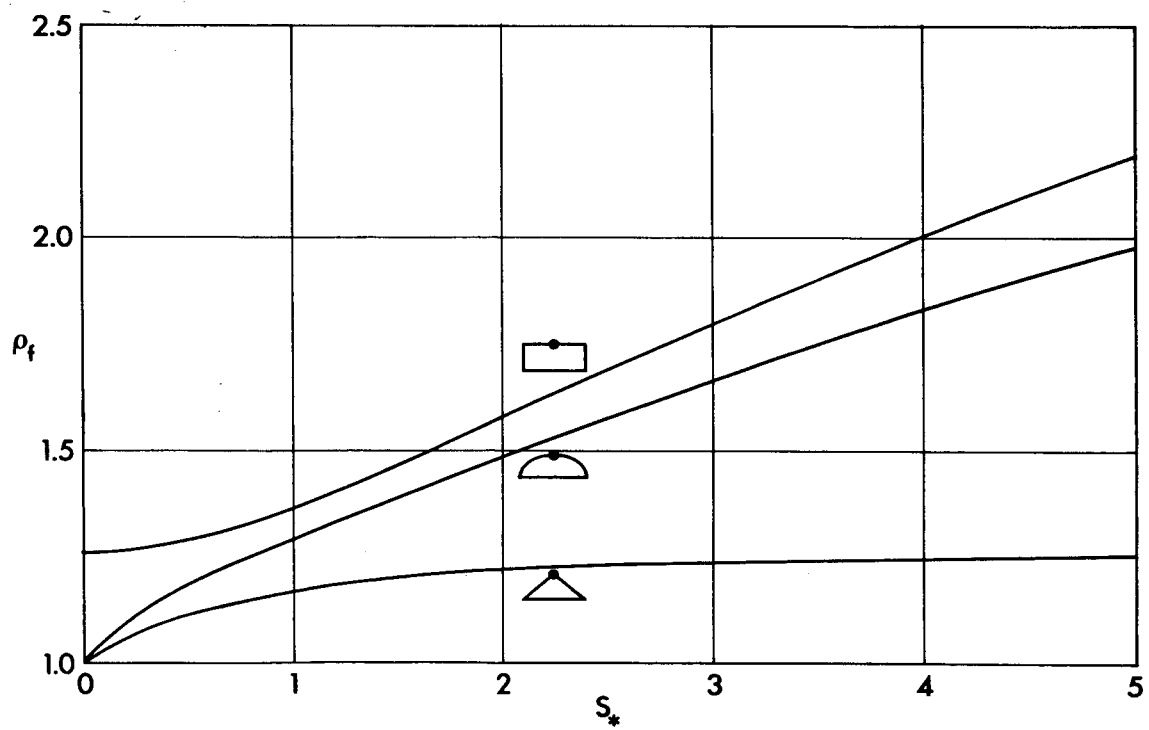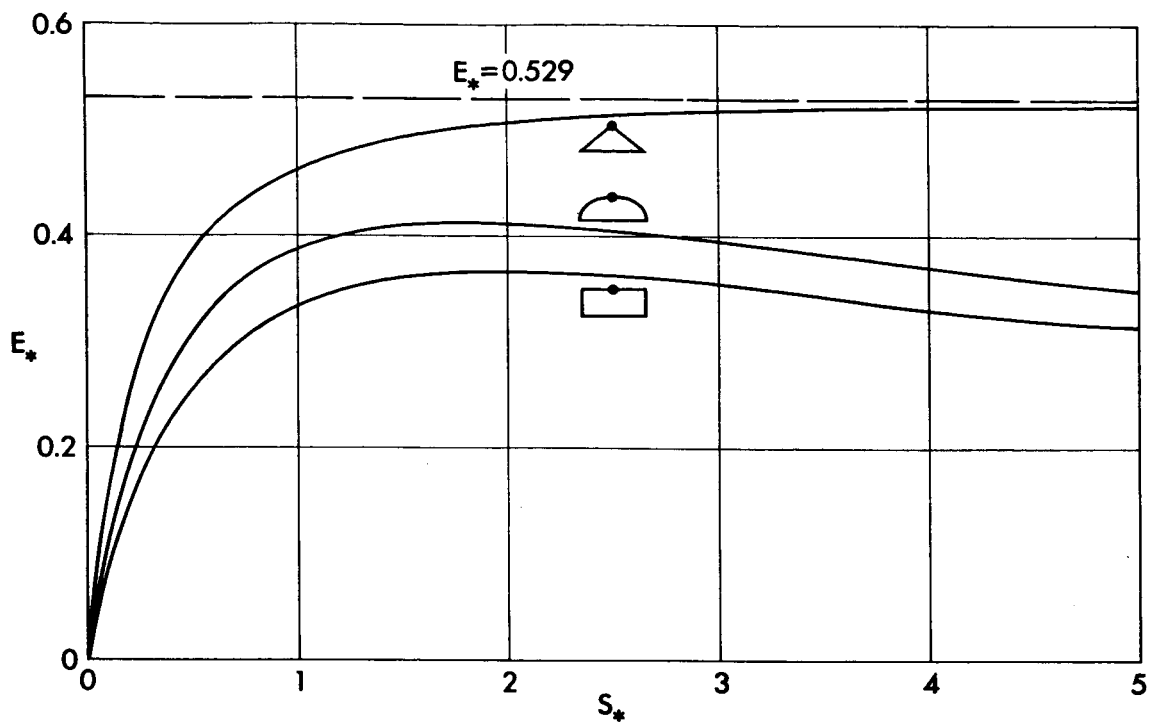
Fig. 9   Final radius.

Fig. 10   Lift-to-drag ratio.
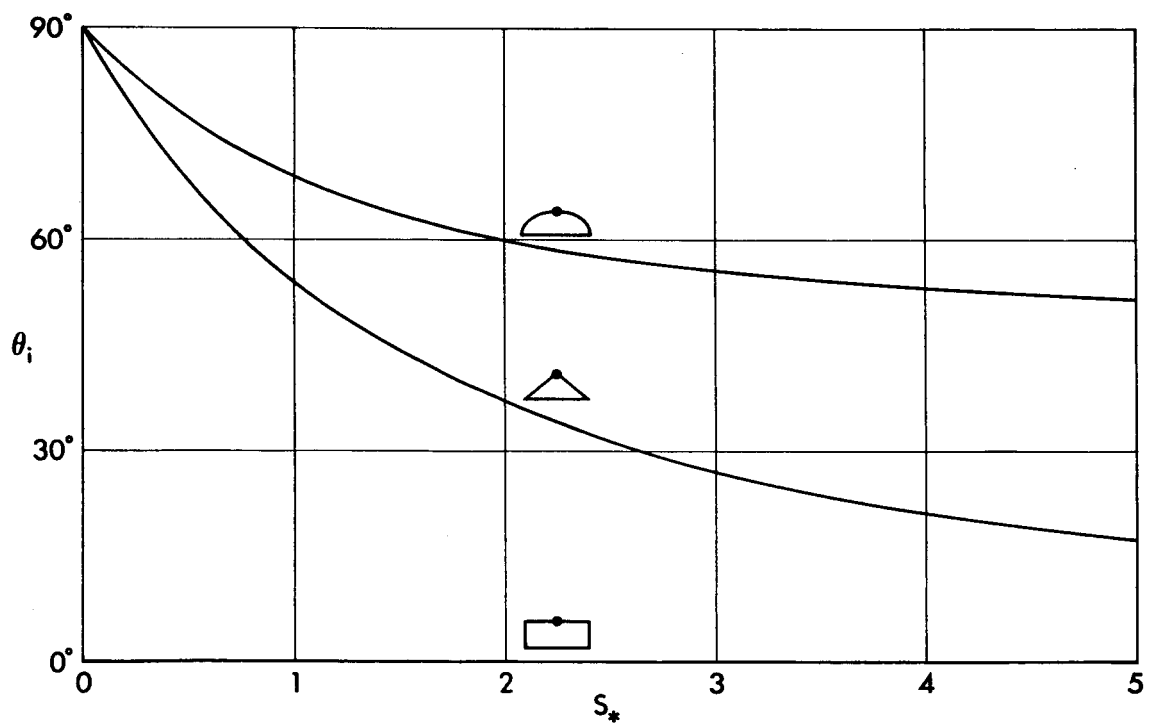
Fig. 11   Initial angle.
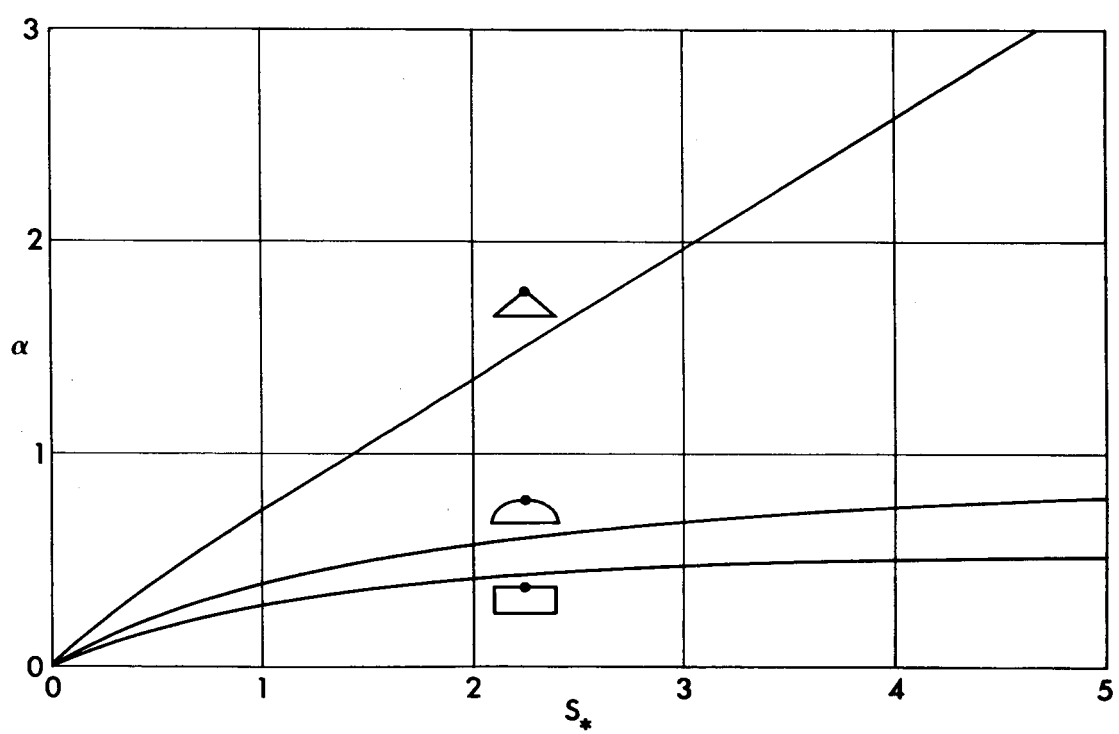
Fig. 12   Elongation ratio.
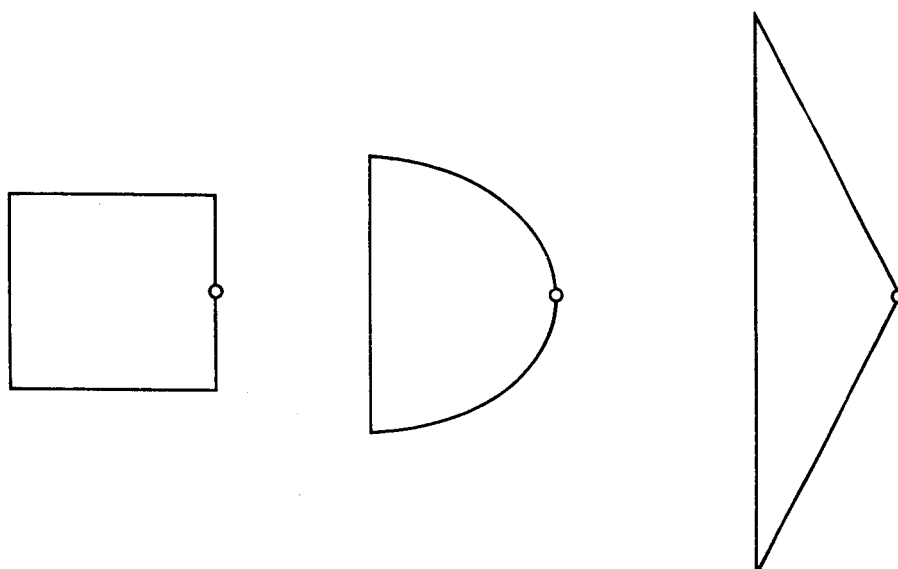
Fig. 13   Optimum contours for S_* = 3.
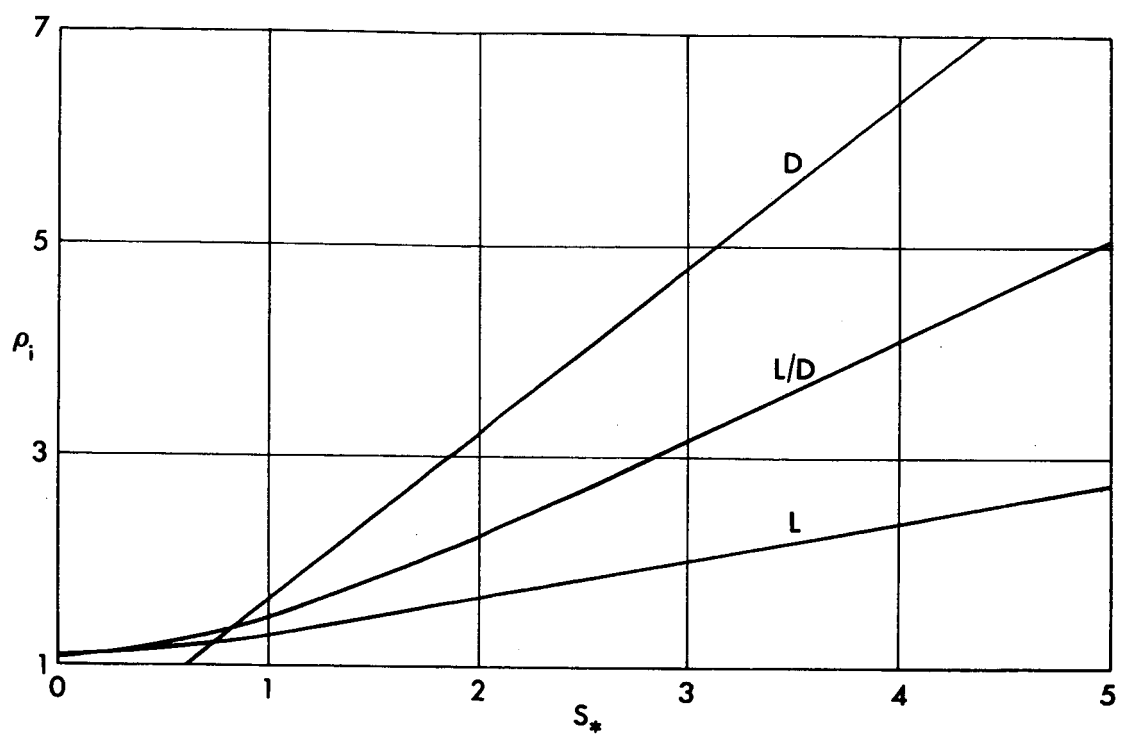
Fig. 14   Initial radius.
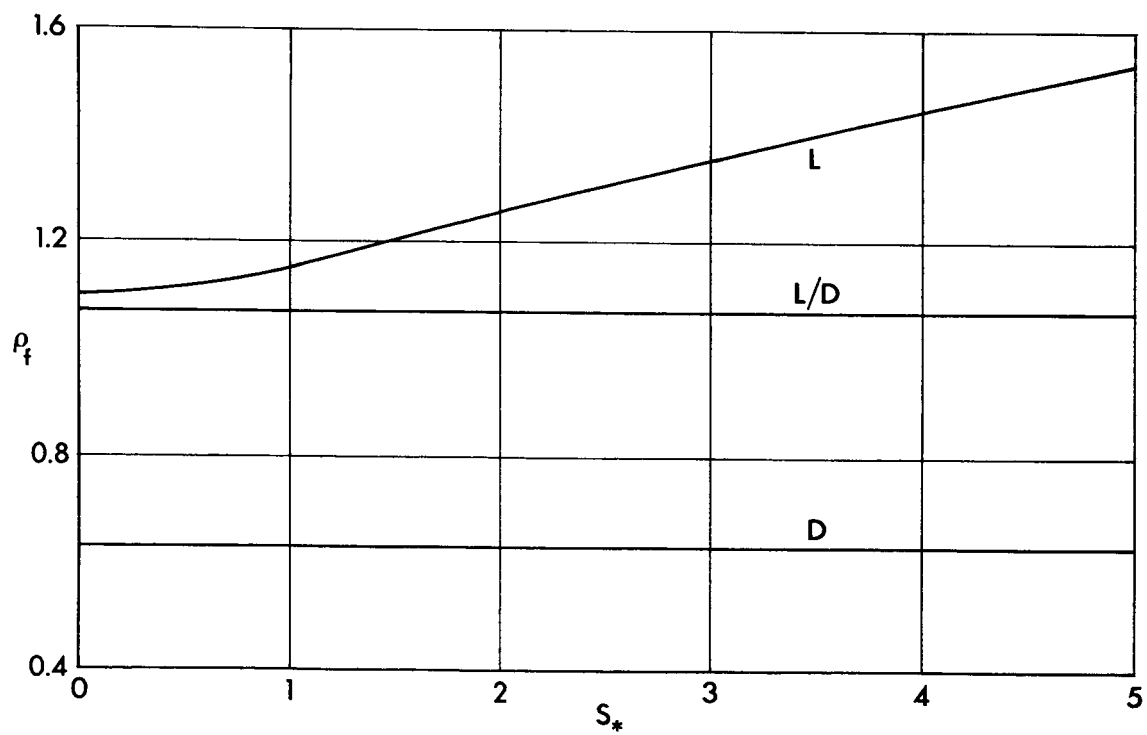
Fig. 15   Final radius.

Fig. 16   Lift-to-drag ratio.

Fig. 17   Initial angle.

Fig. 18   Elongation ratio.

Fig. 19   Optimum contours for $S_* = 3$.

Fig. 20   Initial angle.
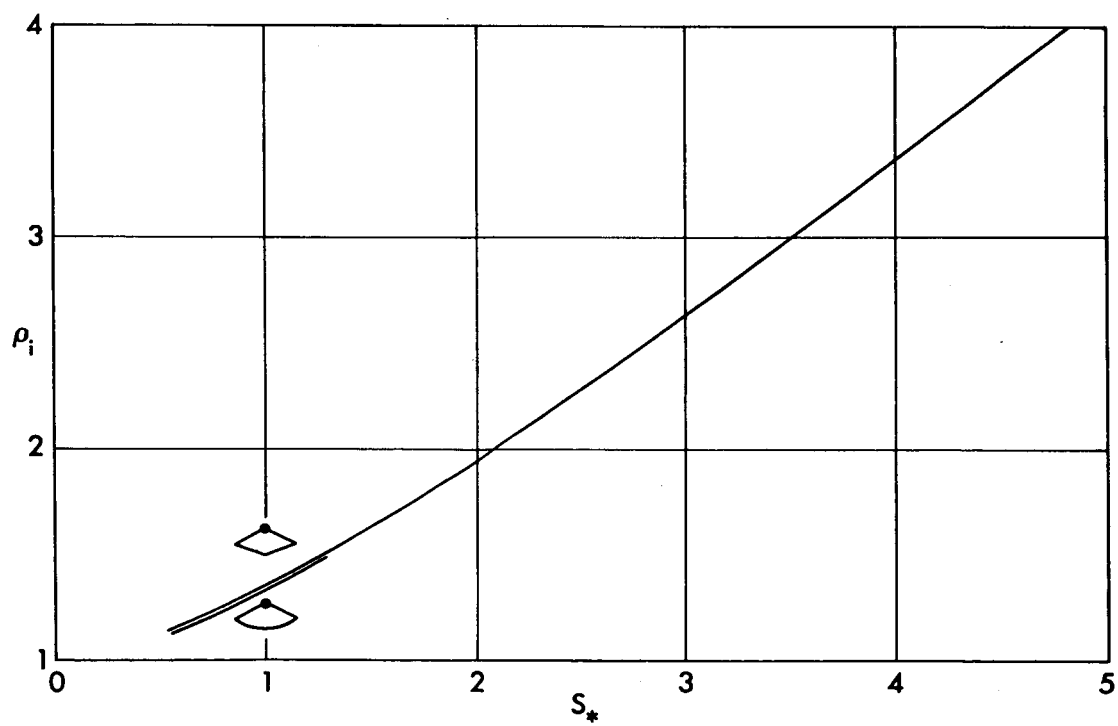
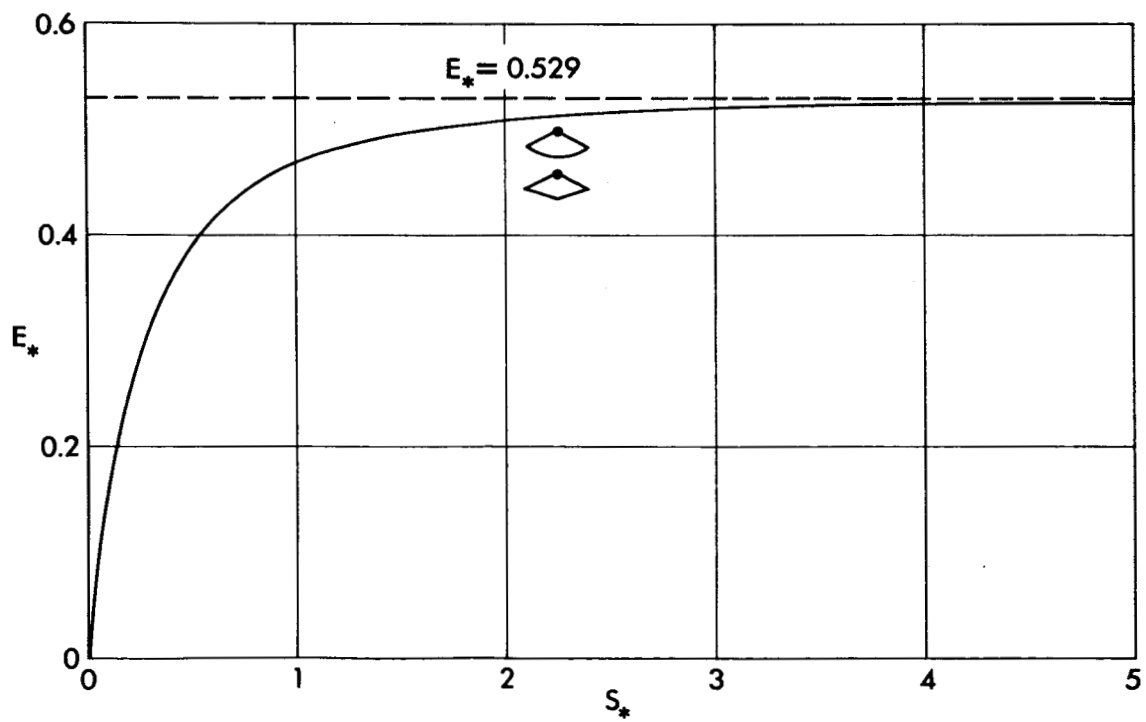Fig. 21   Initial radius.
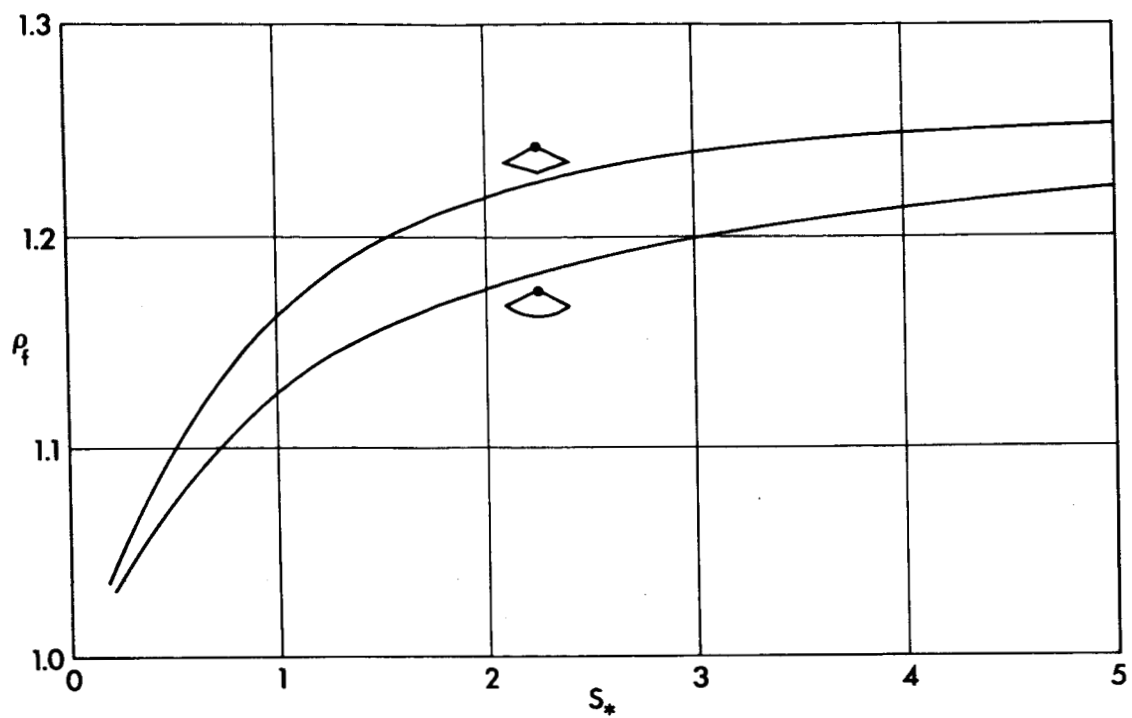
Fig. 22   Final radius.
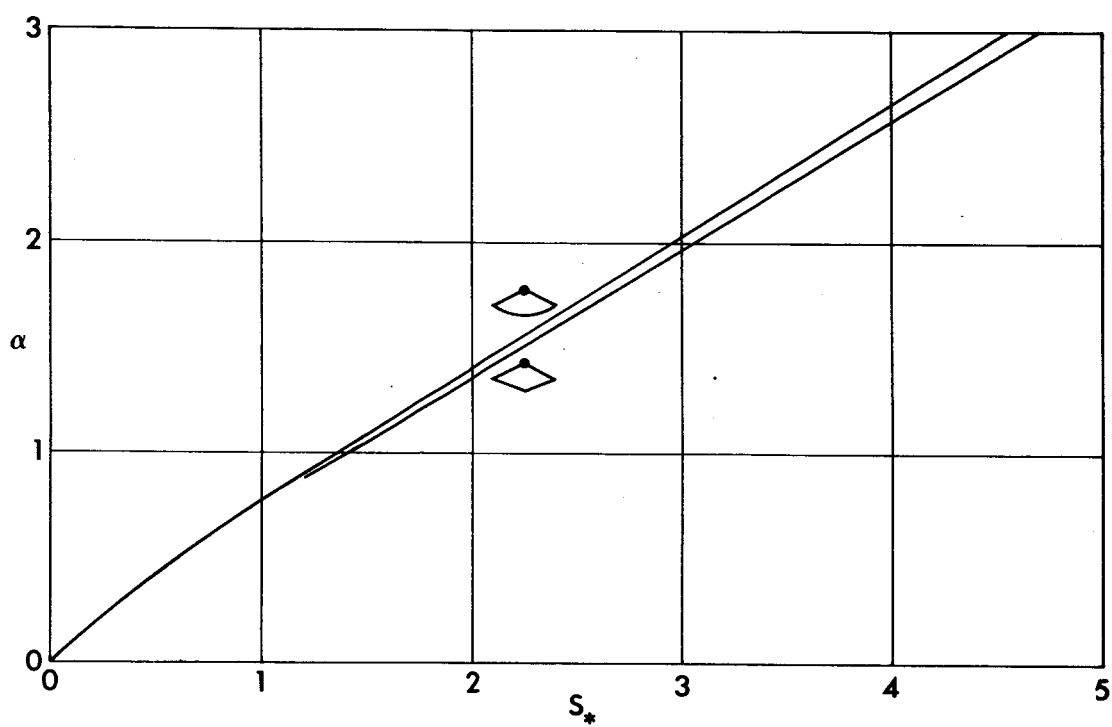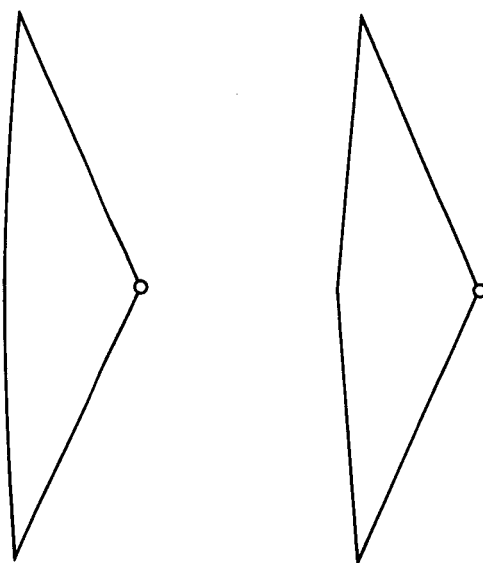

Fig. 23   Lift-to-drag ratio.

Fig. 24   Elongation ratio.

Fig. 25　Optimum contours for $S_* = 3$.